



Characteristics analysis and parameters optimization for the grating eddy current displacement sensor

Hong-li QI, Hui ZHAO^{†‡}, Wei-wen LIU

(Department of Instrument Science and Engineering, Shanghai Jiao Tong University, Shanghai 200240, China)

[†]E-mail: huizhao@sjtu.edu.cn

Received May 9, 2008; Revision accepted Sept. 5, 2008; Crosschecked Apr. 27, 2009

Abstract: The grating eddy current displacement sensor (GECDS) for distance or position measurement used in watertight electronic calipers was described. The sensor relies on repetitive variation of inductance against displacement caused by the change of coupling areas between moving coils and static reflectors. The investigations focused on setting up and utilizing a computer model of the 3D eddy current fields and geometry to analyze causes of the production of measurement blind areas, and to investigate effects of the sensor parameters, such as axial gap between coils and reflectors, reflector length and reflector width on characteristics of the sensor. Simulation results indicated that the sensor has the smallest nonlinearity error of 0.15%, which agrees well with the experimental results.

Key words: Grating eddy current displacement sensor (GECDS), Watertight electronic calipers, Parameters optimization, Nonlinearity

doi:10.1631/jzus.A0820358

Document code: A

CLC number: TH7; TM15

INTRODUCTION

Watertight distance or position measurement devices (such as electronic calipers) are widely used in practically all industrial domains due to some exceptional requirements like resistance to fouling, robustness, watertight, etc. (Jagiella and Fericean, 2002). The sensor, as the main component of a watertight electronic caliper, is mostly of magnetic or inductive type having watertight function in principle at present (Mitutoyo Corporation, 1998; Brown, 2001; Dinulovic *et al.*, 2006).

Magnetic sensors are insensitive to contaminations caused by oil, water and other fluids, but subject to the influence of ferromagnetic particles which are attracted to the magnetized scale (Brown, 2001). Consequently, they must be sealed, encapsulated to prohibit dust from diminishing their effectiveness. Inductive sensors, not only insensitive to contamina-

tions caused by fluids but also to dust and ferromagnetic particles (Mitutoyo Corporation, 1998), have been widely used in watertight electronic calipers now. However, the exciting coil and the pickup coil of inductive sensors are detached and the shape of the pickup coil is relatively complex, which will increase manufacturing and installation costs of the sensors. In this paper, we present a new grating displacement sensor based on the eddy current effect (Zhao *et al.*, 2004a; 2004b). This kind of sensor not only has the function of resistance to liquid in principle but prevents ferromagnetic particles from affecting measurement results as inductive sensors do.

The grating eddy current displacement sensor (GECDS) described in this study is different from traditional eddy current sensors in two main ways. Firstly, the structure of the sensor adopts the form that exciting coil and pickup coil are the same coil, distinct from the form that the above two coils are detached in most previous researches (Kacprzak *et al.*, 2001; Yamada *et al.*, 2004; Dinulovic and Gatzten, 2006).

[‡] Corresponding author

Secondly, the measurement of displacement relies on repetitive variation of coils' inductance caused by the change of coupling areas between moving coils and static reflectors.

When designing a new sensor, it is necessary to have an in-depth analysis on relations between designing parameters and characteristics of the sensor to optimize the sensor. An electromagnetic finite element analysis system can be utilized to reduce our manufacturing cost and development cycle of sensors (Huang *et al.*, 2001). The present simulators of electromagnetic fields have proved to be very capable of delivering most precise results (Jagiella and Fericean, 2002). Due to the complexity of 3D eddy current fields, it is rather difficult and time consuming to set up an accurate mathematic model of the sensor, and infer descriptive equations directly (Sydenham *et al.*, 1995; Juillard *et al.*, 2000). To optimize the sensor, investigate the effects of design parameters on characteristics of the sensor, and especially analyze the nonlinearity of the sensor, we use the Maxwell 3D simulator to set up the computer model of the GECDS and use the model to analyze inductance variation rules of the sensor's coils against displacement. We also investigate effects of the sensor's parameters on sensitivity and nonlinearity and study causes of the production of measurement blind areas. Simulation results prove that the sensor could provide the minimum nonlinearity error of 0.15% over the fixed pitch $\lambda=5$ mm.

SENSORS STRUCTURE AND DESIGN CONSIDERATIONS

Fig.1 shows the schematic representation of the

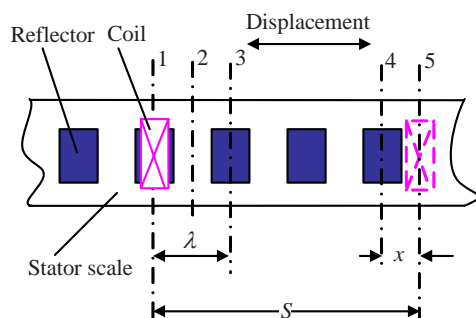


Fig.1 Schematic diagram of the grating eddy current displacement sensor

GECDS. The sensor consists of one coil and a number of reflectors. Reflectors are located on the stator scale with a fixed pitch λ repetitively, while the coil on the moving scale (invisible in Fig.1) is able to move transversely with the moving scale. Coils and reflectors, all made of copper conductor, are nonmagnetic.

When an alternating current with high frequency passes through the coil which moves transversely, coupling areas between the coil and reflectors will be changed, and magnetic flux within the coil will be changed accordingly. This will result in inductance variation of the coil caused by the change of reluctance. Hence the displacement between the coil and reflectors, S , could be converted into inductance variation of the coil. The inductance value can be sensed by tracking the amplitude of current, voltage or frequency which is dependent on the inductance by measurement circuits, so the displacement S can be achieved. The eddy current induced in the reflector has a maximum effect on the coil when the coil situates itself just above the reflector, such as Position 1; inductance of the coil should be minimum at this position. The eddy current induced in the reflector exerts a minimum effect upon the coil when the coil situates itself above the middle position between two reflectors, such as Position 2, where inductance of the coil should be maximum. Inductance of the coil reaches minimum again when the coil moves to the position just above the next reflector (Position 3). Therefore, in a complete cycle (i.e., the fixed pitch λ), inductance of the coil varies from minimum to maximum and then to minimum again. Let the coil move the displacement S and the inductance of the coil vary repetitively. Then the displacement S can be calculated as

$$S=n\lambda+x, \quad (1)$$

where S denotes the displacement between the coil and reflectors, n represents the number of complete cycles, and x indicates the small displacement in one cycle λ .

Fig.2a illustrates the linear variation of the coil's inductance against the pitch λ . The rising and falling segments are symmetrical. A complete cycle of the variation is covered by the displacement which is equal to the length of the fixed pitch λ . However, the linear variation is an idealized approximation of the

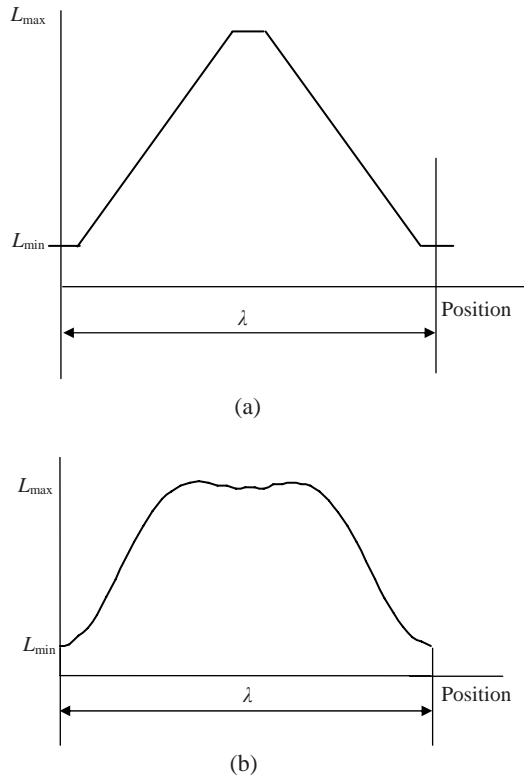


Fig.2 Idealized (a) and experimental (b) inductance variation of the coil in a cycle

inductance variation, as it disregards magnetic field fringing which causes distortions of waveforms (Corda *et al.*, 1999).

In fact the inductance variation of the experimental coil is nonlinear, as illustrated in Fig.2b. The figure indicates that there is a relatively flat waveform peak region (i.e., so called measurement blind areas), which is larger than that in Fig.2a. The cause of the phenomenon is not clear at this stage. According to our analysis, when the coil moves to a certain region between two reflectors, such as Position 2 shown in Fig.1, the eddy current induced in two reflectors near the coil will affect the inductance variation of the coil. The effect of eddy current induced in one reflector is decreased, which makes the inductance of the coil increase. But strengthening eddy current induced in the other reflector makes the inductance of the coil decrease, counteracting the effect of the former reflector. Hence inductance variation is not obvious when the coil moves to certain regions between the two reflectors.

Fig.3a shows the corresponding magnetic field

overlay in three reflectors when the coil is just located above Reflector 2. Fig.3a indicates that the maximum current density vector J_{max} is $1.4489E+004$ (A/m²) in Reflector 2, but J_{max} is $3.1402E-016$ (A/m²) in Reflectors 1 and 3. So effects of the eddy current induced in Reflectors 1 and 3 on the coil can be ignored as compared to those of Reflector 2. Fig.3b illustrates the magnetic field overlay in two reflectors when the coil moves to the site above the middle position between two reflectors. Fig.3b indicates that the current density vector maximum J_{max} is decreased to $7.4920E+003$ (A/m²) in Reflector 2, but J_{max} in Reflector 3 is increased to $7.4920E+003$ (A/m²). Inductance variation of the coil is affected by the eddy current induced in the two reflectors at the same time.

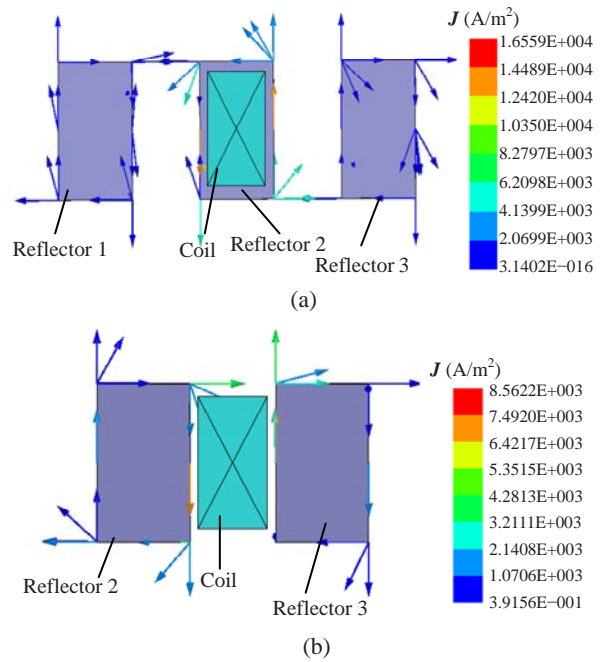


Fig.3 Magnetic field overlays in three (a) and two (b) reflectors

To obtain the desired variation of inductance against displacement and to avoid the production of measurement blind areas, an arrangement with four coils is used. Fig.4 shows the schematic representation of the arrangement. Coils 1 and 2, 3 and 4 are apart from each other by $\lambda/2$ and connected in differential forms respectively to enhance measurement sensitivity and avoid measurement blind areas. Coils 1 and 3, 2 and 4 are apart from each other by $5\lambda/4$ and output cosine and sinusoidal signal separately to measure the small displacement x in one cycle.

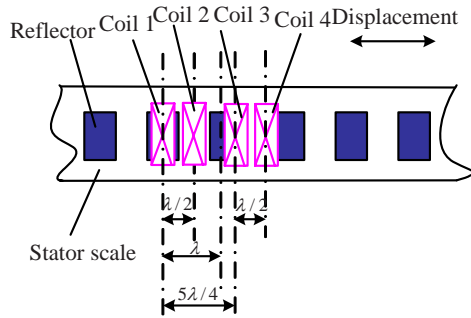


Fig.4 Schematic diagram of the arrangement with four coils

INDUCTANCE WAVEFORM SENSING AND POSITION IDENTIFICATION

The inductance waveform can be sensed by tracking the variation of frequency which is dependent on the inductance variation. As the aim is to achieve a direct relationship between the sensor output signal and displacement, the electrical circuit should be in the form that provides a linear dependence between the output signal and inductance of the coil. Frequency modulation circuit was used. Coils 1, 2 output differential frequency signal f_{12} and coils 3, 4 output differential frequency signal f_{34} . Since coils 1 and 3, 2 and 4 are apart from each other by $5\lambda/4$, waveforms of differential frequency against displacement are shifted in phase for $\lambda/4$.

Fig.5a shows the frequency variation of coils 1 and 2 against the displacement which is equal to the length of two cycles (i.e., 10 mm). The differential frequencies are shown in Fig.5b. Fig.5 indicates that $\lambda/2$ segments of the differential frequency f_{12} have a better sensitivity in MHz/mm than corresponding segments of the original coils and eliminate the blind areas of waveform.

Because approximately the differential frequency curve f_{12} approaches the cosine curve and the differential frequency curve f_{34} draws close to the sinusoidal curve, curves f_{12} and f_{34} can be roughly expressed as

$$f_{12} = A \cos(2\pi x / \lambda), \tag{2}$$

$$f_{34} = A \sin(2\pi x / \lambda). \tag{3}$$

Let the phase angle be

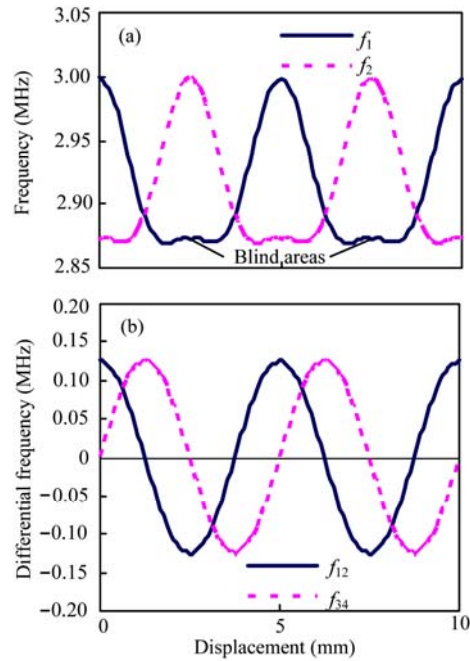


Fig.5 Frequency waveforms. (a) Frequency waveforms of coils 1 and 2; (b) Differential frequency waveforms

$$\varphi = 2\pi x / \lambda, \tag{4}$$

then

$$\varphi = \arctan\left(\frac{f_{34}}{f_{12}}\right) = \arctan\left(\frac{A \sin(2\pi x / \lambda)}{A \cos(2\pi x / \lambda)}\right). \tag{5}$$

Fig.6 illustrates the linear variation of the phase angle φ against the displacement which is equal to the length of two cycles according to Eq.(5). Thus the small displacement x mentioned in Section 2 can be obtained through phase angle φ :

$$x = \lambda \varphi / (2\pi). \tag{6}$$

Assuming n (the numbers of complete cycle λ) has been acquired, displacement S can be calculated by Eq.(1).

SENSOR CONFIGURATIONS AND THE SIMULATION MODEL

Due to the highest inductance density of spiral coil configuration as compared to planar coil (Hamasaki and Ide, 1995), multi-layer planar rectangular spiral coils have been selected in this

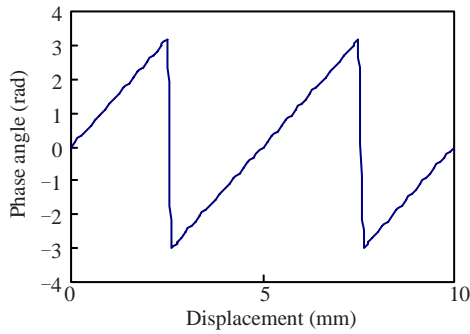


Fig.6 Linear variation between phase angle and displacement

research. The rectangular spiral coils were manufactured using the flexible printed circuit technology; i.e., the coil consists of rectangular spiral copper traces on a substrate. A schematic representation of the multi-layer coils is presented in Fig.7, where the structure was simplified to a stack of only 2-layer of planar spiral coils. The sensor was designed as a 10-layer of planar spiral coils and successive layers were connected by via holes. In the present work, the following configurations were studied: a coil made of 10-layer rectangular 4-turn copper traces. The definition of all parameters of the sensor is presented as follows: a is length of reflector; b is width of reflector; D_1 is length of coil; D_2 is width of coil; d_1, d_2 are inner diameters of the coil; c_1 is thickness of single-layer coil; c_2 is thickness of reflector; h is axial gap between coil and reflector; s is width of the copper traces; t is the gap between copper traces; N is number of turns on per layer; m is number of layers; f is excitation frequency. The experimental sensor has been designed with coils which are excited by sinusoidal alternating current. Parameters of the sensor are: $a=2.5$ mm, $b=4$ mm, $D_1=2.4$ mm, $D_2=4.7$ mm, $c_1=0.03$ mm, $c_2=0.06$ mm, $s=t=0.1$ mm, $N=4$, $m=10$, $h=0.5$ mm, $\lambda=5$ mm, $f=3$ MHz. The inner diameters of the coil $d_1=1$ mm and $d_2=3.3$ mm can be determined by

$$d_1 = D_1 - (2N - 1)(s + t), \quad (7)$$

$$d_2 = D_2 - (2N - 1)(s + t). \quad (8)$$

When setting up the computer model of the sensor, it is necessary to make all parameters of the model approach real design parameters of the sensor to enable the high agreement of simulation results with experimental results in quantity. In this study, the real number of layers $m=10$, which could be

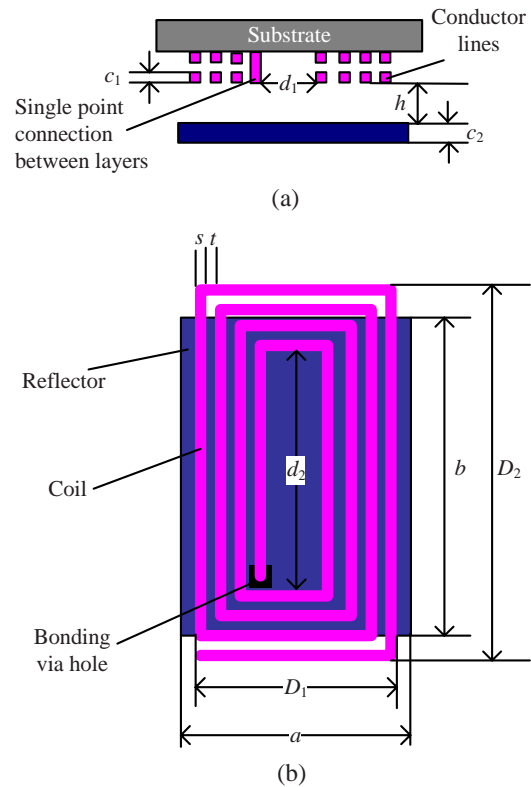


Fig.7 Schematic presentation of multi-layer coil

excessively time-consuming if we set up the model according to the real situation. Therefore, the model with 2-layer coils was used. Inductance variation of 2-layer coils can be obtained through simulation. The relationship between inductance and the number of layers can be achieved through deduction. Inductance variation of 10-layer coils can thus be acquired. Note that the connecting form of different layers coils should ensure the reinforcement of magnetic coupling of coils and two ports of coils should be formed into a closed loop through connecting line in the course of building the simulation model. When all other parameters of rectangular coils with rectangular cross-section are invariant, inductance L is proportional to the square of the turns of the coil (Theodoulidis and Kriezis, 2002; Ditchburn and Burke, 2005). So inductance of 10-layer coils can be obtained:

$$L_{10} = \left(\frac{10}{2}\right)^2 \cdot L_2 = 25L_2, \quad (9)$$

where L_{10} denotes the inductance of a 10-layer coil

and L_2 the inductance of a 2-layer coil.

As frequency modulation circuit was used, frequency variation of simulation results could be obtained:

$$f = \frac{1}{2\pi\sqrt{LC}}, \quad (10)$$

where the value of C is known, equal to that of real circuit.

The resonance frequency of real circuit was measured. We can obtain the validity of simulation results in comparison with real measured results as shown in Fig.8. Two curves of frequency against displacement have the same variation rules and cycle. A complete variation cycle is 5 mm, which is equal to the length of the pitch λ . Fig.8 shows that the measured frequency is from 2.92 to 3.06 MHz and the simulative frequency from 2.62 to 2.78 MHz, indicating that simulation results are close to measured results in quantity.

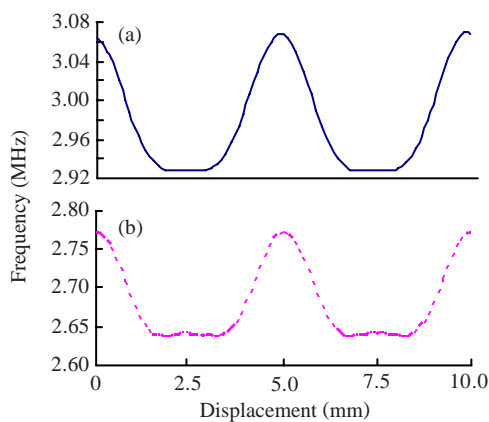


Fig.8 Comparison between (a) measured and (b) simulative results

EFFECTS OF DESIGN PARAMETERS ON THE CHARACTERISTICS OF THE GECDS

Since the profile of inductance waveform directly affects the sensor's linearity, an optimal design needs to be done to minimize the nonlinearity of the sensor. According to our experience in experiments and simulation, the nonlinearity error of the sensor was affected by many parameters of the sensor. In this work, since geometric parameters of the planar rec-

tangular spiral coils are more complex as compared to those of the reflectors, simulation experiments were implemented through changing the parameters of reflectors and the axial gap between coils and reflectors. At the given pitch length and coils parameters, parameters affecting the nonlinearity error were: reflector length a , reflector width b and the axial gap between coils and reflectors h . Here, the thickness of reflectors is 0.06 mm, bigger than the penetration depth of the eddy current. To assess how the three design parameters influence the profile, the inductance waveforms were computed for various sets of parameters using a Maxwell 3D simulator. The criterion used to select parameters was the smallest nonlinearity, expressed in a percentage ratio of the maximum deviation of measured phase angle from the idealized straight line (the angle phase against the displacement line shown in Fig.6) to the span of phase angle variation over the fixed pitch λ .

Effects of design parameters on the inductance and sensitivity of the sensor

The effects of altering the three design parameters on the inductance and sensitivity of the sensor at a fixed pitch ($\lambda=5$ mm) were summarized in Fig.9. The effects of altering reflector length are shown in Fig.9a, indicating that the inductance of the coil at the same position will increase when the reflector length decreases. The reason is that the larger the outer diameter of the coil in comparison with the reflector length is, the wider the axial magnetic overlay will become; on the other hand, the gradient variation becomes smaller, which will cause the decrease of effects on inductance and thus the increase of inductance. Furthermore, Fig.9a shows that the variation of reflector length has a negligible effect on the sensitivity, as can be also seen in Table 1.

The effects of altering h are given in Fig.9b, suggesting that the larger h is, the larger the inductance value of the coil is at the same position. It can be attributed to the fact that the larger h is, the smaller effects on inductance of the coil have and then the inductance will be larger. Furthermore, Fig.9c shows that the larger h is, the smaller the sensitivity becomes, as can be also seen in Table 2.

The effects of altering reflector width are given in Fig.9c. This figure shows that the effects of reflector width variation on inductance have the same

variation rules as reflector length variation when reflector width is less than 4.5 mm, but inductance becomes almost invariable when reflector width exceeds 4.5 mm, as shown in Table 3.

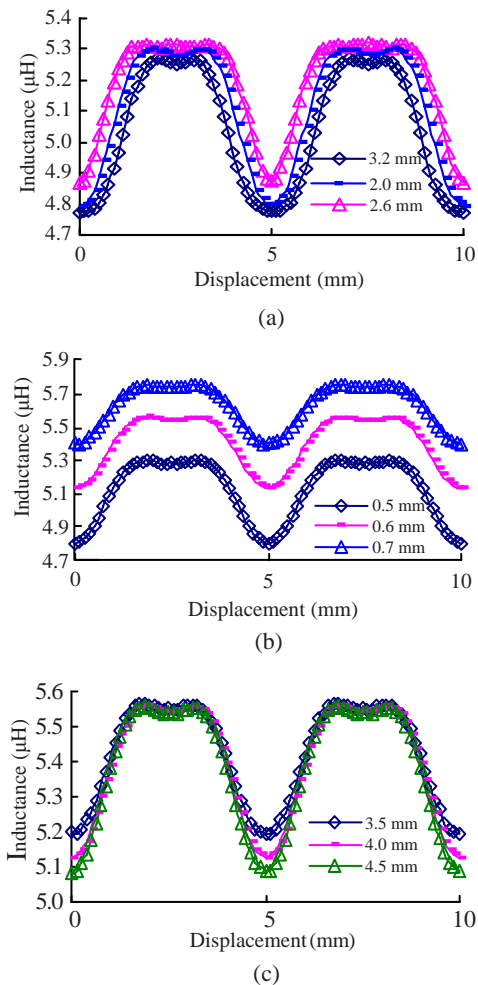


Fig.9 The effects of altering the three design parameters on the inductance and sensitivity of the sensor at a fixed pitch ($\lambda=5$ mm). (a) Reflector lengths; (b) Axial gaps; (c) Reflectors widths

Effects of design parameters on the nonlinearity of the sensor

The effects of altering the three design parameters on the nonlinearity of the sensor at a given pitch ($\lambda=5$ mm) were summed up in Tables 1, 2 and 3. The effects of altering the reflector length are given in Table 1. Table 1 indicates that it is appropriate to select the reflector length at 2.6 mm, which gives the minimum nonlinearity error of 0.38% at the span of inductance variation of 0.510 μ H. Furthermore, the table shows that either increasing or decreasing the

Table 1 Effects of reflector length on nonlinearity

Reflector length (mm)	Span of inductance variation (μ H)	Nonlinearity error (%)
2.0	0.450	2.35
2.4	0.495	0.89
2.5	0.504	0.57
2.6	0.510	0.38
3.0	0.502	1.32
3.2	0.501	2.10

Table 2 Effects of axial gap on nonlinearity at the fixed reflector length (2.6 mm)

Axial gap (mm)	Span of inductance variation (μ H)	Nonlinearity error (%)
0.3	0.6719	1.22
0.4	0.5843	0.85
0.5	0.5036	0.57
0.6	0.4318	0.34
0.7	0.3594	0.45
0.8	0.3056	0.61
0.9	0.2584	0.65
1.0	0.2141	0.75

Table 3 Effects of reflector width on nonlinearity

Reflector width (mm)	Span of inductance variation (μ H)	Nonlinearity error (%)
3.5	0.3719	0.65
4.0	0.4369	0.30
4.3	0.4562	0.24
4.4	0.4637	0.17
4.5	0.4726	0.16
4.6	0.4752	0.18
4.7	0.4780	0.15
5.0	0.4794	0.25

reflector length will increase the nonlinearity error of the sensor.

Table 2 shows that there is an optimum axial gap of 0.6 mm with respect to the minimum nonlinearity error of 0.34%. A reduction of the axial gap below 0.6 mm, though increasing the span of inductance variation (i.e., sensitivity), enlarges nonlinearity of the sensor and raises the cost of manufacturing. Hence, the axis gap of 0.6 mm is considered as an optimum.

The effects of altering reflector width at the fixed reflector length 2.6 mm and axial gap 0.6 mm are given in Table 3. The table indicates that it is appropriate to select the reflector width of 4.7 mm, yielding the minimum nonlinearity of 0.15% at the span of inductance variation of 0.4780 μ H.

According to the above analysis, the sensor has

the smallest nonlinearity error of 0.15% at a fixed pitch $\lambda=5$ mm, reflector length 2.6 mm, reflector width 4.7 mm and axial gap 0.6 mm when all other parameters are invariable. Fig.10 shows the corresponding optimum inductance waveform of two complete cycles. Fig.11 illustrates the corresponding phase angle variation and idealized phase angle straight line against the displacement which is equal to the length of one cycle (from 2.5 to 7.5 mm). As Fig.11 indicates, the optimum phase angle curve overlaps the idealized phase angle straight line well. Fig.12 shows the corresponding nonlinearity error

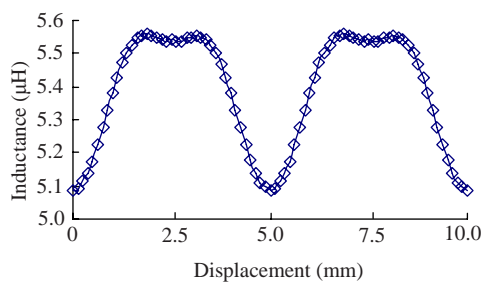


Fig.10 Optimum inductance variation in two complete cycles

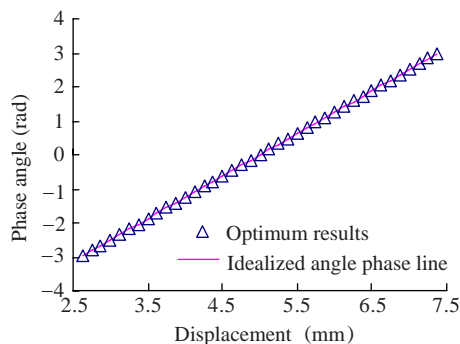


Fig.11 Optimum phase angle variation in one complete cycle

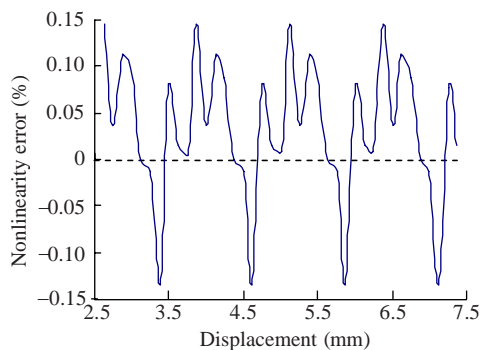


Fig.12 Non-linearity error in one complete cycle

which is expressed in a percentage ratio of the deviation of phase angle from the idealized straight line to the span of phase angle variation (i.e., 2π) of one cycle.

The position errors occurring over the fixed pitch λ are not accumulative, which is an important feature of the GECDS. For instance, the maximum position error, associated with the nonlinearity error of 0.15% over the fixed pitch $\lambda=5$ mm, is 0.0075 mm and independent of the measuring range.

CONCLUSION

This study presented the GECDS for linear position measurement. To eliminate measurement blind areas, the structure of the sensor was arranged so that the phase angle variations of one cycle are linearly proportional to small displacement. To optimize the production sensor, a computer model of the 3D eddy current fields was set up to investigate the effects of such parameters as the axial gap between coils and reflectors, the reflector length and the reflector width on sensitivity and nonlinearity.

The best result obtained was the smallest nonlinearity error of 0.15% over the fixed pitch $\lambda=5$ mm when stricter control was undertaken on the manufacture of the coils and reflectors. Note that the above results were not always optimum. Since each optimal parameter was acquired by assuming the invariance of the other two parameters, this method is not an optimum algorithm and needs to be studied further.

References

- Brown and Sharpe Tesa S.A., 2001. Magnetoresistive Sensor for High Precision Measurements of Lengths and Angles. US Patent, No. 6191578.
- Corda, J., Tayie, J.k.A., Slater, P., 1999. Contactless linear position transducer based on reluctance variation. *IEE Proc.-Electr. Power Appl.*, **146**(6):585-590. [doi:10.1049/ipepa:19990693]
- Dinulovic, D., Gatzten, H.H., 2006. Microfabricated inductive micropositioning sensor for measurement of a linear movement. *IEEE Sensors J.*, **6**(6):1482-1487. [doi:10.1109/JSEN.2006.884439]
- Dinulovic, D., Hermann, D., Fluegge, J., Gatzten, H.H., 2006. Development of a linear micro-inductosyn sensor. *IEEE Trans. Magn.*, **42**(10):2830-2832. [doi:10.1109/TMAG.2006.879141]
- Ditchburn, R.J., Burke, S.K., 2005. Planar rectangular spiral

- coils in eddy-current non-destructive inspection. *NDT & E Int.*, **38**(8):690-700. [doi:10.1016/j.ndteint.2005.04.001]
- Hamasaki, Y., Ide, T., 1995. Fabrication of Multi-Layer Eddy Current Micro Sensors for Non-destructive Inspection of Small Diameter Pipes. Micro Electro Mechanical Systems (MEMS), Proc. IEEE, p.232-237. [doi:10.1109/MEMSYS.1995.472574]
- Huang, L., Rahman, A., Rolph, W.D., Pare, C., 2001. Electromagnetic finite element analysis for designing high frequency inductive position sensors. *IEEE Trans. Magn.*, **37**(5):3702-3705. [doi:10.1109/20.952694]
- Jagiella, M., Fericean, S., 2002. Miniaturized Inductive Sensors for Industrial Applications. Proc. IEEE Sensors, **2**:771-778. [doi:10.1109/ICSENS.2002.1037204]
- Juillard, J., Barmon, B., Berthiau, G., 2000. Simple analytical three-dimensional eddy-current model. *IEEE Trans. Magn.*, **36**(1):258-266. [doi:10.1109/20.822536]
- Kacprzak, D., Taniguchi, T., Nakamura, K., Yamada, S., Iwahara, M., 2001. Novel eddy current testing sensor for the inspection of printed circuit boards. *IEEE Trans. Magn.*, **37**(4):2010-2012. [doi:10.1109/20.951037]
- Mitutoyo Corporation, 1998. Induced Current Absolute Position Transducer Using a Code-track-type Scale and Read Head. US Patent, No. 5841274.
- Sydenham, P.H., Taing, V., Mounsey, D.J., Yu, W.X., 1995. Low-cost, precision, flat inductive sensor. *Measurement*, **15**(3):179-188. [doi:10.1016/0263-2241(94)00048-C]
- Theodoulidis, T.P., Kriezis, E.E., 2002. Impedance evaluation of rectangular coils for eddy current testing of planar media. *NDT & E Int.*, **35**(6):407-414. [doi:10.1016/S0963-8695(02)00008-7]
- Yamada, S., Chomsuwan, K., Fukuda, Y., Iwahara, M., Wakiwaka, H., Shoji, S., 2004. Eddy-current testing probe with spin-valve type GMR sensor for printed circuit board inspection. *IEEE Trans. Magn.*, **40**(4):2676-2678. [doi:10.1109/TMAG.2004.829254]
- Zhao, H., Ma, D.L., Liu, W.W., Yu, P., 2004a. Design of a new inductive grating displacement sensor and application in liquid resistant caliper. *J. Shanghai Jiao Tong Univ.*, **38**(8):1382-1384 (in Chinese).
- Zhao, H., Liu, W.W., Yu, P., Tao, W., 2004b. Summary on water-proof electronic digital caliper. *New Technol. & New Process*, (12):7-10 (in Chinese).